ACS OMEGA

http://pubs.acs.org/journal/acsodf

Article

Investigation of the Influence of Pressure on the Physical Properties and Superconducting Transition Temperature of Chiral Noncentrosymmetric $TaRh_2B_2$ and $NbRh_2B_2$

Mohammad Asrafusjaman, Jakiul Islam, M. Azizar Rahman, and AbuI Kashem Mohammad Akther Hossain*

Cite This: *ACS Omega* 2023, 8, 21813−21822

Read Online

ACCESS | Metrics & More | Article Recommendations

ABSTRACT: $TaRh_2B_2$ and $NbRh_2B_2$ compounds exhibit noncentrosymmetric superconductivity with a chiral structure. Density functional theory-based ab-initio calculations have been executed to analyze the structural properties, mechanical stability, ductility/brittleness behaviors, Debye temperature, melting temperature, optical response to incident photon energy, electronic characteristics, and superconducting transition temperature of chiral $TaRh_2B_2$ and $NbRh_2B_2$ compounds under pressure up to 16 GPa. Both the chiral phases are mechanically stable and exhibit ductile nature under the studied pressure. The maximum value of the Pugh ratio (an indicator of ductile/brittle behaviors) is observed to be 2.55 (for $NbRh_2B_2$) and 2.52 (for $TaRh_2B_2$) at 16 GPa. The lowest value of the Pugh ratio is noticed at 0 GPa for both these chiral compounds. The analysis of reflectivity spectra suggests that both the chiral compounds can be used as efficient reflecting materials in the visible energy region. At 0 GPa, the calculated densities of states (DOSs) at the Fermi level are found to be 1.59 and 2.13 states eV^{-1} per formula unit for $TaRh_2B_2$ and $NbRh_2B_2$, respectively. The DOS values of both the chiral phases do not alter significantly with applied pressure. The shape of the DOS curve of both compounds remains almost invariant with applied pressure. The pressure-induced variation of Debye temperatures of both compounds is observed, which may cause the alternation of the superconducting transition temperature, T_c, with applied pressure. The probable changing of T_c with pressure has been analyzed from the McMillan equation.

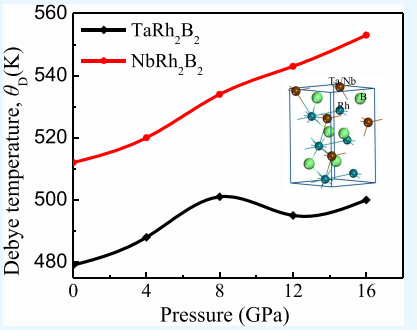

1. INTRODUCTION

The discovery of superconductivity is still fascinating and puzzling to the research community since the beginning of its invention.[1] The researchers are on a thrust to find out a new class of superconductors with attractive features, particularly high-temperature superconductivity. A recent discovery of two Rh-based noncentrosymmetric (NCS) superconductors $TaRh_2B_2$ and $NbRh_2B_2$, with a chiral structure reported by Carnicom and his co-workers,[2] has created a new revolution in the area of superconductivity research. They reported NCS superconductivity with transition temperatures, T_c, 5.8 and 7.6 K for $TaRh_2B_2$ and $NbRh_2B_2$, respectively. Very recently, Islam and his co-authors theoretically verified the low-temperature superconductivity as well as the physical properties of these NCS superconductors.[3] In 2020, the low-symmetry NCS superconductivity has also been revealed in two Ir-based compounds with strong spin-orbit coupling.[4] The inversion symmetry is the general feature of most superconducting materials with the centrosymmetric structure, which maintains the conventional Cooper pairs. However, conventional Cooper pairs do not exist in the case of NCS superconductors due to the shortcoming of inversion symmetry.[2,4] The chiral structure is a crucial addition to the NCS superconductivity in which the superconducting gap function, $\Delta(k)$, the phase has to move either in a clockwise or in a counterclockwise way as k winds in direction to the Fermi surface.[2,5] There are a notable number of experimental investigations that have been accomplished on NCS superconductivity in recent years.[6−11] However, NCS superconductivity with the chiral structure is rare.[3,12,13] For the special feature of the chiral structure, both the Rh-based NCS $TaRh_2B_2$ and $NbRh_2B_2$ superconductors attract massive attention from researchers.[14−17] Mayoh and his coresearchers exhibited the multigap bulk type-II superconductivity in $TaRh_2B_2$ with a higher upper critical field value of 15.2 T, crossing the Pauli limit.[14] Mayoh et al. also justified the bulk type-II superconductivity in $NbRh_2B_2$ with a higher upper critical field along with a T_c of ∼7.46 K.[15] In 2021, Matano and his co-workers verified the NCS superconductivity with

Received: March 3, 2023
Accepted: May 9, 2023
Published: June 6, 2023

antiferromagnetic spin fluctuations in both $TaRh_2B_2$ and $NbRh_2B_2$ chiral compounds.[16] Arumugam et al. investigated the magnetic, flux pinning, and transport characteristics of the NCS $TaRh_2B_2$ superconductor under pressure up to ∼3 GPa and observed the suppressing nature of pinning energy and superconducting properties with applied pressure.[17] From the analysis of flux pinning force, they exhibited the coexistence of both volume and surface pinnings under ambient and high pressure. Both these pinnings in $TaRh_2B_2$ decrease as a result of the attenuation in the pinning centers under external pressure. They calculated the value of T_c under pressures of 0, 1, 1.5, and 2.5 GPa and observed the decreasing trend of T_c with applied pressure in the respective ways 6.02, 5.98, 5.95, and 5.5 K.

From the study of the literature on NCS superconductivity, various fascinating properties of these NCS superconductors have been observed, such as the absence of conventional Cooper pairs,[2] higher upper critical field exceeding Pauli limit,[2,14] multigap superconductivity,[14] antiferromagnetic spin fluctuations,[16] and pressure dependence of T_c.[17]

A theoretical investigation is required to explore the physical characteristics and superconducting behavior of $TaRh_2B_2$ and $NbRh_2B_2$ under pressure. To the best of our extensive survey, the fundamental physical characteristics and superconducting nature of both NCS $TaRh_2B_2$ and $NbRh_2B_2$ superconductors are still not explored theoretically under hydrostatic pressure. Moreover, no experimental/theoretical reports are available on the physical and superconducting characteristics of $NbRh_2B_2$ under pressure. The application of pressure is one of the efficient and clean thermodynamic ways to switch the properties of a compound. Particularly for low-temperature superconductors, the imposed pressure may raise the value of T_c to high-temperature superconductivity. A huge number of research works have been performed under pressure in recent years to achieve high-temperature superconductivity near room temperature.[18−27] Recently, Mariappan and his co-workers investigated the pressure-induced effect on the structural, vortex pinning, and superconducting properties of NCS superconductor Re_6Hf.[28] They reported the decreasing nature of T_c value with applied pressure up to 8 GPa, observed from resistivity measurements. They revealed the monotonic reduction of lattice constants without any structural phase instability up to ∼18 GPa. They also performed density functional theory (DFT) research on the density of states (DOS) under pressure and observed the decreasing affinity of DOS at the Fermi level, which is a possible cause for the reducing value of T_c with increasing pressure. In 2022, Islam and his co-workers also exhibited the pressure-dependent nature of Debye temperature in low-temperature superconductor $CaPd_2P_2$ and predicted the possible variation of T_c with applied hydrostatic pressure using DFT-based ab-initio calculations.[29] These research works motivated us to carry out DFT-based ab-initio calculations on the physical and superconducting characteristics of $TaRh_2B_2$ and $NbRh_2B_2$ under hydrostatic pressure.

Various mechanical parameters such as brittleness/ductility and softness/hardness are required to know about the suitability of a new material for the fabrication of devices. It is also needed to justify the Born elastic stability conditions of a compound to be mechanically stable. The Debye temperature has a linear relation with T_c by the McMillan equation. Therefore, it is also necessary to disclose the Debye temperature value, particularly for superconductors. The melting temperature is also a vital thermodynamic parameter to notify the high-temperature application of a material. The optical functions such as reflectivity, optical absorption, conductivity, and dielectric functions are crucial parameters to predict the application of a compound from various perspectives.

An exhaustive literature survey discloses that the above-mentioned fundamental physical properties of the chiral NCS $TaRh_2B_2$ and $NbRh_2B_2$ superconductors are not yet investigated theoretically under pressure. Therefore, this ab-initio study includes a detailed exploration of the structural, mechanical, thermophysical, optical, electronic, and possible variations of T_c of these two chiral NCS superconductors under pressure up to 16 GPa.

2. COMPUTATIONAL METHODOLOGY

In this study, the DFT-based[30,31] computer code Cambridge Serial Total Energy Package (CASTEP)[32] was conducted to optimize the geometry of $TaRh_2B_2$ and $NbRh_2B_2$ compounds. The physical properties were investigated from the optimized structure of these two Rh-based chiral compounds. The generalized gradient approximation (GGA) suggested by Perdew-Burke-Ernzerhof was taken as the exchange-correlation functional.[33] The electron-ion interactions were performed taking ultrasoft pseudopotential.[34] The Broyden−Fletcher−Goldfarb−Shanno scheme[35] was chosen to make sure of the optimization of crystal structures. The energy cutoff of 750 eV and k-points 16 × 16 × 8 (through Monkhorst−Pack schemes) were chosen for the purpose of geometry optimization along with property simulation.[36] The convergence parameters were picked as follows: energy, 5×10^{-6} eV/atom; maximum stress, 0.02 GPa; maximum displacement, 5×10^{-4} Å; maximum force, 0.01 eV/Å; and strain amplitude, 0.003.

3. RESULTS AND DISCUSSION

3.1. Structural Properties. The chiral compounds $TaRh_2B_2$ and $NbRh_2B_2$ possess a trigonal form with space group $P3_1$ (no. 144). The crystal structure of these chiral compounds is depicted in Figure 1. The calculated values of

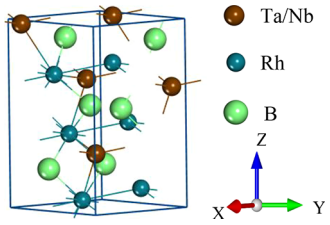

Figure 1. Structural configuration of $TaRh_2B_2$ and $NbRh_2B_2$ compounds.

lattice parameters and cell volume under variant hydrostatic pressures are listed in Table 1. The space between the atoms gets reduced with applied pressure. Consequently, the lattice parameters as well as the unit cell volume show a decreasing trend with increasing pressure. The reduction of the space among the atoms under pressure creates a repulsive effect, which helps to enhance the stiffness of the compound compression under pressure. As this is the first DFT-based theoretical approach of these compounds under pressure, there are no available theoretical data on structural parameters to compare with the present investigations.

https://doi.org/10.1021/acsomega.3c01461
ACS Omega 2023, 8, 21813−21822

Table 1. Pressure-Induced Variation of Lattice Parameters, *a* and *c*, along with Unit Cell Volume, *V*, of $TaRh_2B_2$ and $NbRh_2B_2$

P (GPa)	phase	*a* (Å)	*c* (Å)	*V* (Å^3)	ref.
0 (Exp.)	$TaRh_2B_2$	4.698	8.770	167.63	2
	$NbRh_2B_2$	4.716	8.749	168.51	
0 (GGA)	$TaRh_2B_2$	4.817	8.839	177.62	3
	$NbRh_2B_2$	4.780	8.820	174.52	
0	$TaRh_2B_2$	4.817	8.839	177.60	this study
	$NbRh_2B_2$	4.779	8.821	174.54	
1	$TaRh_2B_2$	4.810	8.829	176.94	this study
1.5	$TaRh_2B_2$	4.804	8.834	176.56	this study
2.5	$TaRh_2B_2$	4.798	8.826	175.91	this study
4	$TaRh_2B_2$	4.792	8.803	175.03	this study
	$NbRh_2B_2$	4.754	8.786	171.95	
8	$TaRh_2B_2$	4.768	8.769	172.67	this study
	$NbRh_2B_2$	4.729	8.754	169.54	
12	$TaRh_2B_2$	4.744	8.744	170.42	this study
	$NbRh_2B_2$	4.707	8.723	167.35	
16	$TaRh_2B_2$	4.724	8.714	168.39	this study
	$NbRh_2B_2$	4.685	8.695	165.30	

3.2. Mechanical Properties. The exploration of elastic constants provides useful information about crystal stiffness, bonding nature, and mechanical stability. The elastic constants are also required to find the elastic moduli of a solid, which are essential to observe the ductile/brittleness nature, machinability, mechanical hardness, and anisotropy indices. The trigonal $TaRh_2B_2$ and $NbRh_2B_2$ compounds possess six different independent elastic constants, C_{11}, C_{12}, C_{13}, C_{14}, C_{33}, and C_{44} (shown in Table 2).

Another stiffness constant C_{66} is calculated using the value of C_{11} and C_{12} with the help of the expression, $C_{66} = \frac{C_{11} - C_{12}}{2}$. The Born mechanical stability parameters without pressure condition are written as follows for the trigonal crystal:[37,38]

$$C_{11} > |C_{12}|,\ C_{44} > 0,$$
$$C_{13}^2 < \frac{1}{2}C_{33}(C_{11} + C_{12}),$$
$$C_{14}^2 < \frac{1}{2}C_{44}(C_{11} - C_{12}) \equiv C_{44}C_{66} \quad (1)$$

Both the NCS $TaRh_2B_2$ and $NbRh_2B_2$ compounds justify the stability parameters, certifying mechanical stability.[3] The mechanical stability of these two chiral compounds under pressure has not been investigated earlier. Therefore, it is required to check the mechanical stability under pressure. The elastic constants are calculated at 1, 1.5, 2.5, 4, 8, 12, and 16 GPa for $TaRh_2B_2$ and at 4, 8, 12, and 16 GPa for $NbRh_2B_2$. The Born mechanical stability criteria have a modified form for the trigonal crystal under pressure as follows:[39,40]

$$(C_{11} - P) > 0;\ (C_{33} - P) > 0;\ (C_{44} - P) > 0$$
$$(C_{11} - P) > |C_{12} + P|$$
$$(C_{11} + C_{12})(C_{33} - P) > 2(C_{13} + P)^2$$
$$(C_{11} - C_{12} - 2P)(C_{44} - P) > 2 \quad (2)$$

Both the chiral compounds also satisfy the stability criteria under the applied pressures, confirming the mechanical stability. All elastic constants of both $TaRh_2B_2$ and $NbRh_2B_2$ exhibit positive values, but a negative value of C_{14} arises for $NbRh_2B_2$ with and without external pressure. However, the positive value of C_{14} is not a criterion to be mechanically stable. Natural quartz, corundum, and many other trigonal compounds also possess a negative value of C_{14}.[40−48] The impact of hydrostatic pressure on C_{14} is significant for the $NbRh_2B_2$ compound. Such small values of C_{14} operate the symmetry regards to be hexagonal.[47] The external pressure also influences the C_{14} value (shows up and down) in the case of $TaRh_2B_2$. The maximum value is observed to be 3.63 GPa at 8 GPa, and the minimum value is found to be 1.35 GPa at 16 GPa hydrostatic pressure for $TaRh_2B_2$. The gradual increasing trend of other stiffness constants (C_{11}, C_{12}, C_{13}, C_{14}, C_{33}, C_{44}, and C_{66}) is observed for $NbRh_2B_2$ under pressure, which implies that the compound becomes stiffer with the increase of pressure. For $TaRh_2B_2$, the up and down of the various stiffness constant values are observed under the studied pressure but do not exhibit any drastic change with applied pressure. From Table 2, it can be observed that the values of unidirectional stiffness constants C_{11} and C_{33} are notably higher compared to the shear stiffness constant C_{44} under the studied pressure for both compounds, which indicates that the shear deformation should be easier compared to the axial compression. The difference between the stiffness constants C_{12} and C_{44} is

Table 2. Pressure-Induced Variation of Elastic Constants C_{ij} of $TaRh_2B_2$ and $NbRh_2B_2$

P (GPa)	phase	C_{11}	C_{12}	C_{13}	C_{14}	C_{33}	C_{44}	C_{66}
0 (ref 3.)	$TaRh_2B_2$	429.60	163.81	195.17	1.59	439.52	120.36	132.90
	$NbRh_2B_2$	398.33	163.88	196.23	−1.63	429.85	108.02	117.23
0	$TaRh_2B_2$	429.85	162.74	196.02	2.61	437.44	119.22	132.90
	$NbRh_2B_2$	396.92	162.61	196.20	−1.38	429.60	108.24	117.16
1	$TaRh_2B_2$	428.85	162.45	201.75	1.60	440.93	116.37	133.2
1.5	$TaRh_2B_2$	441.18	166.86	201.01	1.80	446.21	104.24	137.16
2.5	$TaRh_2B_2$	437.47	161.04	209.82	1.789	451.20	103.72	138.22
4	$TaRh_2B_2$	463.70	176.81	211.21	3.43	462.25	119.43	143.45
	$NbRh_2B_2$	423.96	177.36	213.26	−1.08	452.59	109.48	123.30
8	$TaRh_2B_2$	486.04	191.83	226.80	3.63	489.78	131.37	147.11
	$NbRh_2B_2$	450.33	190.93	227.99	−0.19	480.45	117.79	129.70
12	$TaRh_2B_2$	515.31	202.37	243.96	2.09	510.88	116.47	156.47
	$NbRh_2B_2$	479.46	205.73	244.57	−0.38	502.56	119.92	136.87
16	$TaRh_2B_2$	538.99	216.29	260.61	1.35	532.96	117.57	161.35
	$NbRh_2B_2$	504.55	219.97	260.38	−0.19	526.91	124.93	142.29

https://doi.org/10.1021/acsomega.3c01461
ACS Omega 2023, 8, 21813−21822

Table 3. Pressure-Induced Variation of Voigt Bulk Modulus B_V, Reuss Bulk Modulus B_R, Mean Bulk Modulus, B (GPa), Voigt Shear Modulus B_V, Reuss Shear Modulus B_R, Mean Shear Modulus, G (GPa), Young's Modulus, E (GPa), Pugh Ratio, B/G, Poisson's Ratio, ν, and Universal Anisotropy Factor, A^U

P (GPa)	phase	B_V	B_R	B	G_V	G_R	G	E	B/G	ν	A^U
0 (ref 3.)	$TaRh_2B_2$	267.45	266.90	267.17	124.36	123.85	124.11	322.40	2.15	0.30	0.023
	$NbRh_2B_2$	259.91	258.49	259.20	111.33	110.97	111.15	291.75	2.33	0.31	0.022
0	$TaRh_2B_2$	267.41	266.87	267.14	123.88	123.25	123.57	321.18	2.16	0.30	0.023
	$NbRh_2B_2$	259.28	257.74	258.51	111.29	110.92	111.11	291.55	2.32	0.31	0.022
1	$TaRh_2B_2$	270.06	269.18	269.62	122.03	121.21	121.62	317.17	2.22	0.30	0.037
1.5	$TaRh_2B_2$	274.04	273.55	273.79	119.77	117.88	118.83	311.43	2.30	0.31	0.082
2.5	$TaRh_2B_2$	276.39	275.08	275.73	118.83	116.61	117.72	309.16	2.34	0.31	0.099
4	$TaRh_2B_2$	287.57	287.23	287.40	129.16	128.01	128.58	335.69	2.24	0.31	0.046
	$NbRh_2B_2$	278.70	277.28	277.99	114.90	114.36	114.63	302.33	2.43	0.32	0.028
8	$TaRh_2B_2$	305.86	305.42	305.64	136.40	135.72	136.05	355.43	2.25	0.31	0.026
	$NbRh_2B_2$	297.21	295.76	296.49	122.00	121.54	121.77	321.32	2.43	0.32	0.024
12	$TaRh_2B_2$	324.67	324.27	324.47	134.63	132.15	133.39	351.94	2.43	0.32	0.096
	$NbRh_2B_2$	316.80	315.60	316.20	126.44	125.77	126.10	333.92	2.50	0.32	0.030
16	$TaRh_2B_2$	342.88	342.47	342.67	137.53	134.68	136.10	363.92	2.52	0.32	0.107
	$NbRh_2B_2$	335.27	334.09	334.68	131.45	130.74	131.10	347.87	2.55	0.33	0.031

specified as the Cauchy pressure (CP), which implies the mechanical failure mode of a crystal.[49] The negative (positive) value of CP indicates the brittle (ductile) nature of a compound. Both the chiral compounds exhibit the positive value of CP under the studied pressure, revealing their ductile nature. The Voigt−Reuss−Hill schemes[50−52] are used to estimate the elastic moduli. The bulk modulus (B), shear modulus (G), and Young's modulus (E) are calculated using the equations presented elsewhere.[3] The mechanical parameters of both these compounds are displayed in Table 3, which includes the Voigt bulk modulus (B_V), Reuss bulk modulus (B_R), Voigt shear modulus (G_V), Reuss shear modulus (G_R), B, G, E, Pugh ratio (B/G), Poisson's ratio (ν), and universal anisotropy factor (A^U).

The value of G is a good indicator of the strength of a compound. Both the Rh-based compounds exhibit $G < B$. Hence, the mechanical failure mode of these compounds might be dominated by the applied shear factor. B is a useful parameter that assesses the ability of a compound to withstand volume change under external pressure, whereas G evaluates the resistance to shape change (plastic deformation). From Table 3, $TaRh_2B_2$ can be considered as a hard chiral compound compared to $NbRh_2B_2$ under the studied pressure as $TaRh_2B_2$ exhibits a higher value of G. It can be slightly difficult to modify the volume of $TaRh_2B_2$ compared to $NbRh_2B_2$ under stress because the $TaRh_2B_2$ compound shows the higher value of B in comparison with $NbRh_2B_2$ under the investigated pressure. Similar behavior is also observed in the case of longitudinal tensile resistance (observed from the value of E) under the studied pressure. Moreover, the values of E are higher compared to the other two elastic moduli for both the chiral compounds under the studied pressure, which reveals that both compounds are more effective in withstanding longitudinal tensile stress.

The Pugh ratio and Poisson's ratio are two useful parameters to exhibit the ductility/brittleness nature of a compound. The values lower (higher) than 1.75 (for Pugh ratio) and 0.26 (for Poisson's ratio) indicate a brittle (ductile) nature.[53,54] Both the compounds exhibit ductile nature under the studied pressure as they possess Pugh ratio and Poisson's ratio values higher than the critical values. Moreover, pressure-dependent behavior of ductility is observed for both the chiral compounds. $NbRh_2B_2$ exhibits a higher value of Pugh ratio compared to $TaRh_2B_2$, indicating the high ductility nature of the $NbRh_2B_2$ compound under the investigated pressures. The maximum value of the Pugh ratio is observed to be 2.55 (for $NbRh_2B_2$) and 2.52 (for $TaRh_2B_2$) at 16 GPa. The minimum value of the Pugh ratio is found without applied pressure for both compounds. These results suggest that the ductility behavior of these compounds can be improved further by applying a hydrostatic pressure. To observe the pressure effect on ductility clearly, the variation of the Pugh ratio of $TaRh_2B_2$ and $NbRh_2B_2$ under pressure has been presented in Figure 2a,b, respectively.

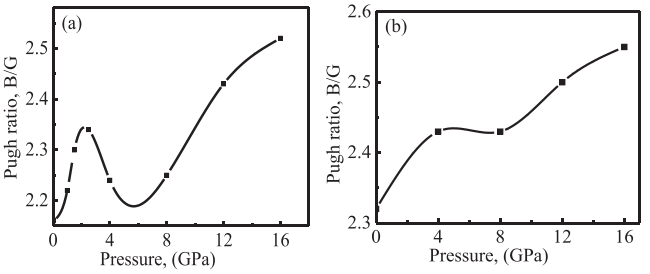

Figure 2. Variation of Pugh ratio of (a) $TaRh_2B_2$ and (b) $NbRh_2B_2$ with applied pressure.

The Poisson's ratio is also an efficient parameter to demonstrate the existence of interatomic forces in the atoms of the solid. The Poisson's ratio value between 0.25 and 0.50 notifies the existence of central force in the atoms of the crystal, and outside this range indicates noncentral forces.[55] Both the chiral NCS phases exhibit a Poisson's ratio value within the range of 0.25 and 0.50 under the pressures, revealing the presence of strong central forces among the atoms of these compounds.

It is required to observe the anisotropy nature of a compound to reveal the direction-dependent behavior of the fundamental properties. The probability of generating microfractures in a compound under stress can be known from the analysis of the anisotropy factor. The universal anisotropy factor is a significant parameter to reveal the anisotropy nature. It can be observed using the following equation:[42]

https://doi.org/10.1021/acsomega.3c01461
ACS Omega 2023, 8, 21813−21822

Table 4. Pressure-Induced Variation of Density ρ, Longitudinal Sound Velocity v_l, Transverse Sound Velocity v_t, Average Sound Velocity v_m, Debye Temperature θ_D, and Melting Temperature T_m of $TaRh_2B_2$ and $NbRh_2B_2$ Compounds

pressure (GPa)	phase	ρ (g/cc)	v_l (m/s)	v_t (m/s)	v_m (m/s)	θ_D (K)	T_m (K)
0 (ref 3.)	$TaRh_2B_2$	11.45	6147	3292	3680	480	2302
	$NbRh_2B_2$	9.14	6676	3487	3904	512	2194
0	$TaRh_2B_2$	11.45	6141	3285	3672	479	2300
	$NbRh_2B_2$	9.14	6670	3486	3904	512	2189
1	$TaRh_2B_2$	11.50	6127	3252	3638	475	2302
1.5	$TaRh_2B_2$	11.52	6125	3211	3592	470	2347
2.5	$TaRh_2B_2$	11.56	6118	3191	3571	468	2343
4	$TaRh_2B_2$	11.62	6284	3326	3720	488	2439
	$NbRh_2B_2$	9.28	6813	3514	3939	520	2305
8	$TaRh_2B_2$	11.78	6430	3398	3802	501	2547
	$NbRh_2B_2$	9.41	6983	3597	4032	534	2426
12	$TaRh_2B_2$	11.94	6486	3342	3743	495	2666
	$NbRh_2B_2$	9.54	7125	3635	4078	543	2546
16	$TaRh_2B_2$	12.08	6587	3356	3760	500	2770
	$NbRh_2B_2$	9.65	7266	3685	4134	553	2658

$$A^U = \frac{5G_V}{G_R} + \frac{B_V}{B_R} - 6 \geq 0. \quad (3)$$

The value of A^U is equal to zero for isotropic crystals, and any fluctuations from zero indicate anisotropic nature. From Table 3, it can be noticed that the studied chiral compounds are anisotropic under the investigated pressures but show less anisotropic nature as the values are closer to zero.

3.3. Melting Temperature and Debye Temperature.

The melting temperature, T_m, reflects the strengths of atomic bond in a solid. The higher value of T_m indicates the suitability of a substance in high-temperature applications. T_m is calculated using the stiffness constants C_{11} and C_{33} via the following expression:[56]

$$T_m = 354 + 4.5\,\frac{2C_{11} + C_{33}}{3} \quad (4)$$

Form Table 4, it can be observed that T_m of $TaRh_2B_2$ decreases slightly at 2.5 GPa. However, T_m of both chiral compounds increases with the increase of applied pressure from 4 to 16 GPa. $TaRh_2B_2$ exhibits higher T_m compared to $NbRh_2B_2$ under the studied pressure.

Therefore, applied pressure can be a fruitful approach to enhance the T_m of these chiral compounds. The higher T_m of $TaRh_2B_2$ indicates that the Ta-containing chiral compound is stiffer in comparison with the $NbRh_2B_2$ compound, which also supports the analysis of the elastic moduli. These trigonal chiral compounds possess a higher T_m (and consequently stiffer) compared with many other trigonal superconductors.[40,47,48] The variation of T_m of $TaRh_2B_2$ and $NbRh_2B_2$ compounds with applied pressure has been displayed in Figure 3a,b, respectively.

The Debye temperature, θ_D, of a solid is a highly significant parameter from many perspectives as it has a connection with various thermophysical indicators such as specific heat, lattice vibration, thermal expansion, and T_m of a solid. Particularly for superconducting materials, the θ_D has a direct linear connection with T_c. The maximum frequency mode of vibrations of a solid depends on the value of θ_D. The θ_D can be estimated in various ways. The calculation of θ_D using average sound velocity (calculated from elastic moduli) is regarded as one of the standard ways, and the required equations are follows:[57]

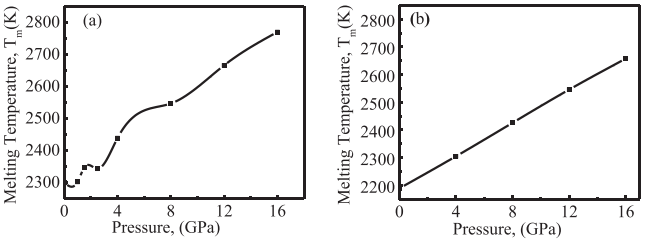

Figure 3. Variation of melting temperature of (a) $TaRh_2B_2$ and (b) $NbRh_2B_2$ under pressure.

$$\theta_D = \frac{h}{k_B}\left[\frac{3n}{4\pi}\left(\frac{N_A\rho}{M}\right)\right]^{1/3} v_m \quad (5)$$

$$v_m = \left[\frac{1}{3}\left(\frac{2}{v_t^3} + \frac{1}{v_l^3}\right)\right]^{-1/3} \quad (6)$$

$$v_l = \left(\frac{3B + 4G}{3\rho}\right)^{1/2} \quad (7)$$

$$v_t = \left(\frac{G}{\rho}\right)^{1/2} \quad (8)$$

where v_t, v_l, v_m, k_B, M, N_A, ρ, h, and n stands for transverse sound velocity, longitudinal sound velocity, mean sound velocity, Boltzmann constant, molecular weight, Avogadro's number, density, Planck constant, and atom number in the molecule, respectively. The calculated values of ρ, v_t, v_l, v_m, T_m, and θ_D under various hydrostatic pressures are displayed in Table 4. From Table 4, it can be observed that θ_D of $TaRh_2B_2$ decreases gradually with the increase of pressure up to 2.5 GPa, which might be the reason for the reducing value of T_c up to this pressure as reported in the literature.[17] This pressure-dependent value of θ_D strongly supports the previous analysis of pressure-induced decreasing trend of T_c up to 2.5 GPa.[17] However, further increase of pressure increases the value of θ_D of the $TaRh_2B_2$ compound up to 8 GPa, and then θ_D remains almost invariant with applied pressure up to 16 GPa. In the case of $NbRh_2B_2$, θ_D shows increasing trend with increasing pressure (with a step of 4 GPa), and the maximum value is

https://doi.org/10.1021/acsomega.3c01461
ACS Omega 2023, 8, 21813−21822

observed to be 552 K at 16 GPa. The pressure-induced variation of θ_D of the $TaRh_2B_2$ and $NbRh_2B_2$ compounds has been depicted in Figure 4a,b, respectively.

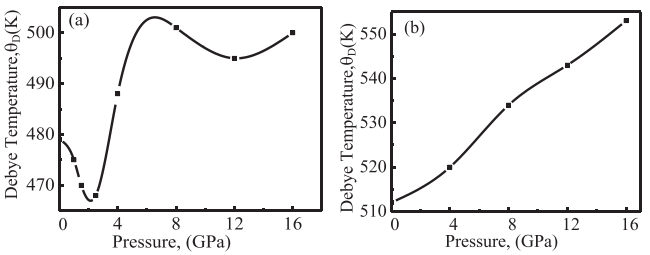

Figure 4. Variation of Debye temperature of (a) $TaRh_2B_2$ and (b) $NbRh_2B_2$ under pressure.

From Figure 4, it can be noticed that θ_D of $NbRh_2B_2$ exhibits a somewhat higher-pressure dependent behavior compared to that of $TaRh_2B_2$. The pressure-dependent value of θ_D is a result of the pressure-induced variation of the elastic constants as well as the sound velocities. We believe this pressure study would be useful enough for designing experimental research project to reveal the pressure-induced variation of T_c along with other physical properties.

3.4. Optical Properties. The study of optical properties is required to observe the material's behavior to the incident photon energy. The analysis of optical behaviors helps to disclose the potential application of a material in optical device applications. The imposed external pressure can alter the properties of a material. The pressure-induced variation of the physical properties can expand the application of a material for diverse perspectives. Therefore, we have calculated various optical parameters such as the reflectivity $R(\omega)$, absorption coefficient $\alpha(\omega)$, real $\sigma_1(\omega)$ and imaginary $\sigma_2(\omega)$ parts of optical conductivity, and real $\varepsilon_1(\omega)$ and imaginary $\varepsilon_2(\omega)$ parts of dielectric functions of the chiral NCS $TaRh_2B_2$ and $NbRh_2B_2$ compounds under pressure. A plasma energy of 6 eV was inserted to analyze the optical functions, and a value in the range of 2−10 eV is recommended for use in a metallic system.

The potentiality of a material as a reflector can be known from the analysis of its reflectivity profile. The pressure-induced reflectivity spectra of $TaRh_2B_2$ and $NbRh_2B_2$ are presented in Figure 5a,b, respectively. The reflectivity spectra do not exhibit significant change with applied pressure without an exception at 16 GPa for $TaRh_2B_2$. At 16 GPa, $TaRh_2B_2$ shows very higher reflectivity curve with a sharp peak in the visible energy zone, but the curve shape is similar to other applied pressures. Both the compounds show a notable peak in

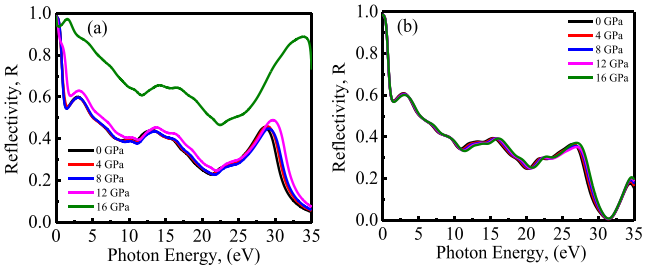

Figure 5. Pressure-induced variation of the reflectivity profile of (a) $TaRh_2B_2$ and (b) $NbRh_2B_2$ compounds.

the visible region under the studied pressure, which implies the suitability of these compounds in practical device as reflectors.

The absorption coefficient provides an idea about the energy-absorbing capability of a material while passing through it. The absorption profiles of $TaRh_2B_2$ and $NbRh_2B_2$ compounds under pressure are displayed in Figure 6a,b,

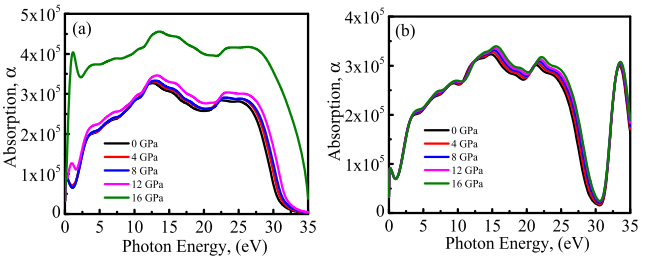

Figure 6. Pressure-induced variation of the absorption profile of (a) $TaRh_2B_2$ and (b) $NbRh_2B_2$ compounds.

respectively. The absorption profiles of both compounds also do not exhibit a notable change with applied pressure, without a larger variation at 16 GPa for the $TaRh_2B_2$ compound. The absorption curves of both $TaRh_2B_2$ and $NbRh_2B_2$ compounds generate at zero photon energy, which is a general behavior of the metallic system.[3] The absorption spectra increase with the increase of photon energy and reach the peak position at ∼12 eV of photon energy for $TaRh_2B_2$ and at ∼15 eV of photon energy for $NbRh_2B_2$.[3]

Figure 7a,b depicts the pressure-induced real part of the optical conductivity (σ_1) profiles of $TaRh_2B_2$ and $NbRh_2B_2$

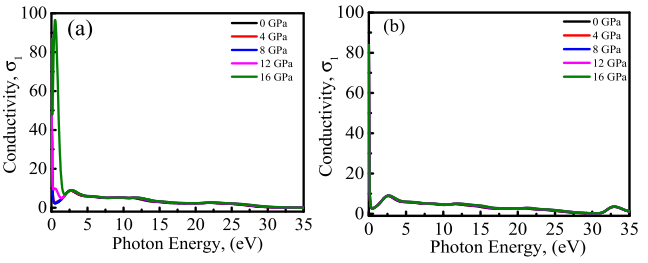

Figure 7. Real part of the optical conductivity (σ_1) of (a) $TaRh_2B_2$ and (b) $NbRh_2B_2$ under pressure.

compounds, respectively. Figure 8a,b illustrates the pressure-induced imaginary part of the optical conductivity (σ_2) profiles of $TaRh_2B_2$ and $NbRh_2B_2$ compounds, respectively. The optical conductivity of a material relies on the photon absorption. The optical conductivity initiates at zero photon energy and becomes nearly flat over a wide extent of photon

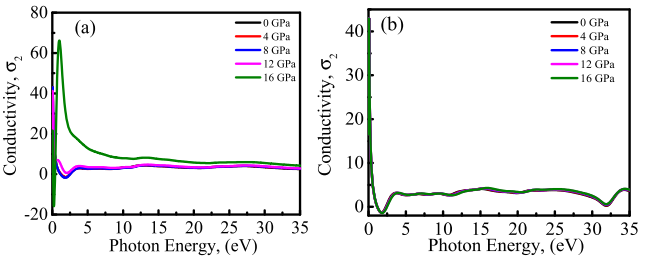

Figure 8. Imaginary part of the optical conductivity (σ_2) of (a) $TaRh_2B_2$ and (b) $NbRh_2B_2$ under pressure.

https://doi.org/10.1021/acsomega.3c01461
ACS Omega 2023, 8, 21813−21822

energy. The application of hydrostatic pressure also does not exhibit notable effect on the optical conductivity spectra of these chiral compounds without an exception at 16 GPa for $TaRh_2B_2$. The starting of optical conductivity at zero photon energy and the behavior of conductivity spectra ensure the strong metallic character of these compounds, verifying the analysis of the optical absorption profile along with other optical functions and electronic properties.

The real part ε_1 of the dielectric function of $TaRh_2B_2$ and $NbRh_2B_2$ under pressure is displayed in Figure 9a,b,

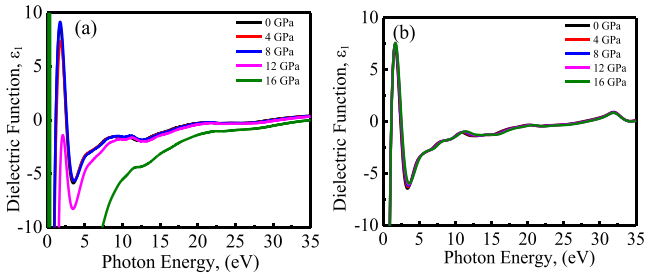

Figure 9. Real part of the dielectric function (ε_1) of (a) $TaRh_2B_2$ and (b) $NbRh_2B_2$ under pressure.

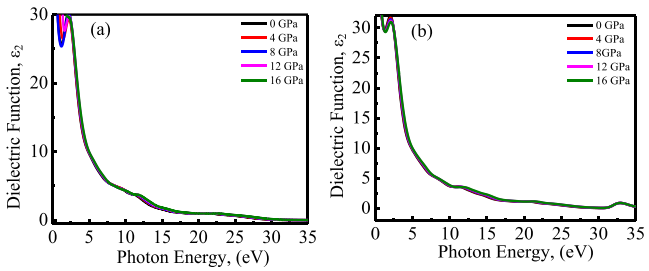

Figure 10. Imaginary part of the dielectric function (ε_2) of (a) $TaRh_2B_2$ and (b) $NbRh_2B_2$ under pressure.

respectively. Figure 10a,b shows the pressure-induced imaginary part (ε_2) of the dielectric function of $TaRh_2B_2$ and $NbRh_2B_2$, respectively. The ε_2 is connected with optical absorption behavior.[3] The ε_1 of both compounds exhibits $\varepsilon_1 < 0$ at zero photon energy and also in the low photon energy region, revealing the metallic feature of these chiral compounds. At 16 GPa, the ε_1 of $TaRh_2B_2$ shows larger variation with other applied pressures, which also supports the analysis of other optical functions. The ε_1 of both chiral compounds tends to reach unity, whereas the ε_2 shows a very low value in the high photon energy region (above ~30 eV). This result suggests that both the chiral phases are anticipated to act as transparent substances in the high photon energy region.[3]

3.5. Electronic Properties. The study of the electronic band structure and DOS provides a clear understanding about the optical response of a material to incident photon energy. The electronic structure of a material mostly relies on the characteristics of valence and conduction electrons. The characteristics of these electrons can be described through the study of their energy dispersion toward different *k*-space directions, namely, Γ-A-H-K-Γ-M-L-H within the Brillouin zone. The band structure of the chiral compounds is exhibited for 0 and 16 GPa along various *k*-space directions within the Brillouin zone. The band structure of $TaRh_2B_2$ at 0 and 16 GPa is displayed in Figure 11a,b, respectively.

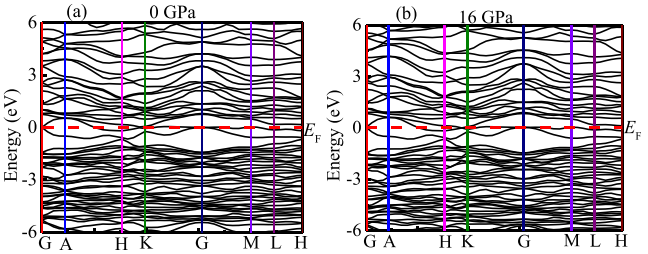

Figure 11. Electronic band structure of $TaRh_2B_2$. (a) 0 GPa and (b) 16 GPa.

Figure 12a,b illustrates the band structure of $NbRh_2B_2$ at 0 and 16 GPa, respectively. The horizontal broken red line below

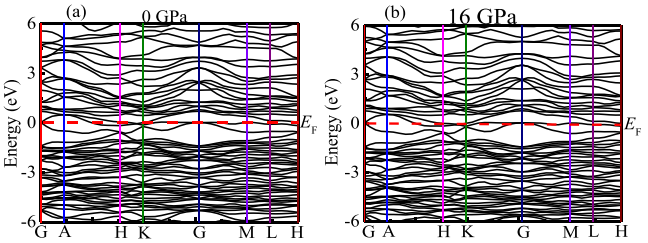

Figure 12. Electronic band structure of $NbRh_2B_2$. (a) 0 GPa and (b) 16 GPa.

the conduction band (CB) and above the valence band (VB) at zero of energy axis depicts the Fermi level (E_F). Here, the CB and VB clearly crosses the E_F at varying dispersion energies with and without applied pressure. Such electronic band energy behavior of a material indicates the metallic nature.

The variation of DOSs of $TaRh_2B_2$ and $NbRh_2B_2$ compounds with applied pressure has been depicted in Figure 13a,b, respectively. The DOS profile provides a further clear

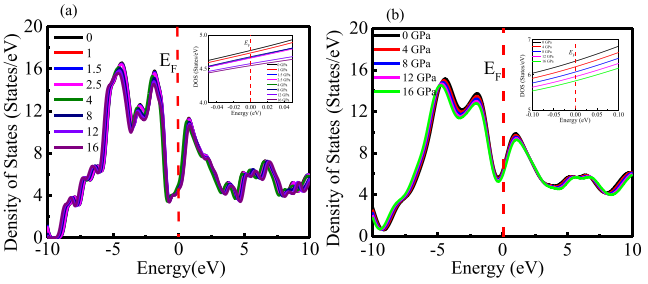

Figure 13. DOS profile of (a) $TaRh_2B_2$ and (b) $NbRh_2B_2$ compounds under pressure.

understanding about the electronic band structure. At 0 GPa, the observed DOSs at E_F are 1.59 and 2.13 states eV^{-1} per formula unit for $TaRh_2B_2$ and $NbRh_2B_2$, respectively, which reveal a reasonable agreement with previous experimental and theoretical reports.[2,3] The DOS value at E_F does not change largely with applied pressure. From the McMillan equation, it can be said that the value of T_c of these compounds under the studied pressure is largely dependent on the variation of θ_D with applied pressure.

3.6. Superconducting Properties. $TaRh_2B_2$ and $NbRh_2B_2$ exhibit low-temperature superconductivity observed

https://doi.org/10.1021/acsomega.3c01461
ACS Omega 2023, 8, 21813−21822

in previous study with $T_c \sim 5.8$ K for the Ta-containing compound and 7.6 K for the Nb-containing compound.[2] The pressure-induced variation of T_c can be predicted from the McMillan equation,[58]

$$T_c = \frac{\theta_D}{1.45}\exp\left[-\frac{1.04\,(1+\lambda)}{\lambda - \mu^*(1+0.62\lambda)}\right] \quad (9)$$

where λ and μ^* indicate the electron−phonon coupling constant and the Coulomb pseudo-potential, respectively.[18] μ^* is estimated using the value of TDOS at the E_F, $N(E_F)$, through the following equation:[59,60]

$$\mu^* = 0.26\frac{N(E_F)}{1+N(E_F)} \quad (10)$$

The value of μ^* taken in the range 0.10−0.15 is physically reasonable.[61] The value of TDOS at E_F of both chiral compounds changes slightly with applied pressure. Therefore, the imposed pressure may not have a large impact on the value of μ^*. λ can be written as

$$\lambda = N(E_F)V_{e-ph}$$

where, $V_{e\text{-}ph}$ stands for the electron−phonon interaction energy.[29,48] Therefore, the variation of λ with applied pressure can be interpreted with the variation of $N(E_F)$ and $V_{e\text{-}ph}$ with applied pressure. It is exhibited in Figure 13 that the applied pressures do not have a large impact on $N(E_F)$. Therefore, the pressure-induced variation of λ will largely depend on the possible pressure effect in $V_{e\text{-}ph}$. In the McMillan equation, if we consider a fixed value of λ of these chiral compounds, then the value of T_c might be largely influenced by the variation of θ_D with applied pressure because θ_D has a linear connection with T_c through the McMillan equation. For the $TaRh_2B_2$ superconductor, the value of θ_D decreases with applied pressure up to 2.5 GPa. Therefore, the value of T_c of $TaRh_2B_2$ should be decreased under pressure up to 2.5 GPa according to the McMillan equation. The decreasing trend of T_c of $TaRh_2B_2$ with applied pressure up to 2.5 GPa was observed in a previous study.[17] Therefore, the present theoretical analysis strongly supports the reported experiment results,[17] carrying reliability of the present investigation. θ_D of $TaRh_2B_2$ increases at 4 and 8 GPa applied pressures. Therefore, it can be predicted that the T_c of $TaRh_2B_2$ may increase at such high pressures. In the case of $NbRh_2B_2$, the value of θ_D increases with increasing applied pressure from 4 to 16 GPa. The pressure-induced increasing trend of θ_D of the chiral NCS $NbRh_2B_2$ superconductor indicates that the value of T_c of this superconductor may increase with the increase of applied pressure. The pressure-induced variation of θ_D along with the possible variation of T_c was also reported on other superconducting materials.[29,48] We believe that this theoretical study in the presence of applied pressure on the chiral NCS superconductors would be useful enough for future experimental observations to verify the pressure-induced variation of the physical characteristics of materials.

4. CONCLUSIONS

The DFT calculations have been performed using the CASTEP module to investigate the structural properties, mechanical performance, thermodynamical behavior, electronic band structure, optical functions, and superconducting behavior of chiral NCS $TaRh_2B_2$ and $NbRh_2B_2$ compounds under variant hydrostatic pressures up to 16 GPa. The present calculated structural parameters at 0 GPa agrees well with previous experimental and theoretical reports, carrying reliability of this study. The unit cell volume of both the compounds decreases smoothly with increasing applied pressure. Both the chiral compounds satisfy the mechanical stability conditions under the studied pressure. The analysis of elastic moduli indicates the soft nature of $NbRh_2B_2$ compared to $TaRh_2B_2$ as $NbRh_2B_2$ possesses lower values of elastic moduli in comparison with $TaRh_2B_2$ under the studied pressure. The Rh-based chiral compounds show a ductile nature (revealed from the Pugh ratio and the Poisson's ratio) under the studied pressure, and their ductility exhibit pressure-dependent behavior. The observed melting temperature of $TaRh_2B_2$ is higher compared to that of $NbRh_2B_2$ under the studied pressures. The melting temperatures of both the chiral compounds increase with the increase of applied pressure from 4 to 16 GPa. This result suggests that applications of these compounds in high-temperature technologies can be further improved applying external pressure. Both these NCS superconductors show a notable reflectivity peak in the visible region. The optical absorption and conductivity of both the compounds start at zero photon energy, which is an expected behavior for a metallic system. The analysis of optical functions justifies the results of the electronic structure. The Debye temperature of both the superconductors varies with applied pressure, which can propagate the value of T_c. The Debye temperature of $TaRh_2B_2$ decreases with applied pressure up to 2.5 GPa as the Debye temperature has a linear relation with T_c. Therefore, the decreasing trend of T_c of the $TaRh_2B_2$ compound is expected up to 2.5 GPa. This result strongly supports the experimental results reported by Arumugam et al., and they observed the decreasing trend of T_c with applied pressure up to 2.5 GPa. We observe the increasing trend of Debye temperature of $TaRh_2B_2$ at 4 and 8 GPa and then almost invariant at 12 and 16 GPa. In the case of $NbRh_2B_2$, the Debye temperature shows an increasing trend with applied pressure. This may cause the variation of T_c with applied pressure, and there is a possibility for an increase in the value of T_c under pressure.

AUTHOR INFORMATION

Corresponding Author

Abul Kashem Mohammad Akther Hossain − *Department of Physics, Bangladesh University of Engineering and Technology, Dhaka 1000, Bangladesh;* orcid.org/0000-0002-0394-167X; Email: akmhossain@phy.buet.ac.bd

Authors

Mohammad Asrafusjaman − *Department of Physics, Bangladesh University of Engineering and Technology, Dhaka 1000, Bangladesh*

Jakiul Islam − *Department of Physics, Bangladesh University of Engineering and Technology, Dhaka 1000, Bangladesh;* orcid.org/0000-0002-6113-5879

M. Azizar Rahman − *Department of Physics, Bangladesh University of Engineering and Technology, Dhaka 1000, Bangladesh*

Complete contact information is available at: https://pubs.acs.org/10.1021/acsomega.3c01461

Notes

The authors declare no competing financial interest.

https://doi.org/10.1021/acsomega.3c01461
ACS Omega 2023, 8, 21813−21822

■ ACKNOWLEDGMENTS

This work was funded by the Research and Innovation Centre for Science and Engineering-RISE, Project ID: 2021-01-012, Bangladesh University of Engineering and Technology, Dhaka-1000, Bangladesh.

■ REFERENCES

(1) Onnes, H. K. The Resistance of Pure Mercury at Helium Temperatures. In *Proceedings Koninklijke Akademie van Wetenschappen te Amsterdam*, 1911; Vol. *13*, p. 1274.
(2) Carnicom, E. M.; Xie, W.; Klimczuk, T.; Lin, J.; Górnicka, K.; Sobczak, Z.; Ong, N. P.; Cava, R. J. $TaRh_2B_2$ and $NbRh_2B_2$: Superconductors with a chiral noncentrosymmetric crystal structure. *Sci. Adv.* **2018**, *4*, 7969.
(3) Islam, J.; Rahman, M. A.; Hossain, A. A. Physical and Superconducting Properties of Chiral Noncentrosymmetric $TaRh_2B_2$ and $NbRh_2B_2$: A Comprehensive DFT Study. *ACS Appl. Electron. Mater.* **2022**, *4*, 143−1152.
(4) Górnicka, K.; Gui, X.; Wiendlocha, B.; Nguyen, L. T.; Xie, W.; Cava, R. J.; Klimczuk, T. $NbIr_2B_2$ and $TaIr_2B_2$−New low symmetry noncentrosymmetric superconductors with strong spin−orbit coupling. *Adv. Funct. Mater.* **2021**, *31*, No. 2007960.
(5) Kallin, C.; Berlinsky, J. Chiral superconductors. *Rep. Prog. Phys.* **2016**, *79*, No. 054502.
(6) Kozelj, P.; Juckel, M.; Amon, A.; Prots, Y.; Ormeci, A.; Burkhardt, U.; Brando, M.; Leithe-Jasper, A.; Grin, Y.; Svanidze, E. Non-centrosymmetric superconductor $Th_4Be_{33}Pt_{16}$ and heavy-fermion $U4Be_{33}Pt_{16}$ cage compounds. *Sci. Rep.* **2021**, *11*, 22352.
(7) Khasanov, R.; Gupta, R.; Das, D.; Amon, A.; Leithe-Jasper, A.; Svanidze, E. Multiple-gap response of type-I noncentrosymmetric BeAu superconductor. *Phys. Rev. Res.* **2020**, *2*, No. 023142.
(8) Khasanov; Gupta, R.; Das, D.; Leithe-Jasper, A.; Svanidze, E. Single-gap versus two-gap scenario: Specific heat and thermodynamic critical field of the noncentrosymmetric superconductor BeAu. *Phys. Rev. B* **2020**, *102*, No. 014514.
(9) Beare, J.; Nugent, M.; Wilson, M. N.; Cai, Y.; Munsie, T. J. S.; Amon, A.; Leithe-Jasper, A.; Gong, Z.; Guo, S. L.; Guguchia, Z.; Grin, Y.; Uemura, Y. J.; Svanidze, E.; Luke, G. M. μ SR and magnetometry study of the type-I superconductor BeAu. *Phys. Rev. B* **2019**, *99*, No. 134510.
(10) Amon, A.; Svanidze, E.; Cardoso-Gil, R.; Wilson, M. N.; Rosner, H.; Bobnar, M.; Schnelle, W.; Lynn, J. W.; Gumeniuk, R.; Hennig, C.; Luke, G. M.; Borrmann, H.; Leithe-Jasper, A.; Grin, Y. Noncentrosymmetric superconductor BeAu. *Phys. Rev. B* **2018**, *97*, No. 014501.
(11) Smidman, M.; Salamon, M. B.; Yuan, H. Q.; Agterberg, D. F. Superconductivity and spin orbit coupling in non-centrosymmetric materials: A review. *Rep. Prog. Phys.* **2017**, *80*, No. 036501.
(12) Yuan, H. Q.; Agterberg, D. F.; Hayashi, N.; Badica, P.; Vandervelde, D.; Togano, K.; Sigrist, M.; Salamon, M. B. S-wave spin triplet order in superconductors without inversion symmetry: Li_2Pd_3B and Li_2Pt_3B. *Phys. Rev. Lett.* **2006**, *97*, No. 017006.
(13) Nishiyama, M.; Inada, Y.; Zheng, G. Q. Spin triplet superconducting state due to broken inversion symmetry in Li_2Pt_3B. *Phys. Rev. Lett.* **2007**, *98*, No. 047002.
(14) Mayoh, D. A.; Hillier, A. D.; Götze, K.; Paul, D. M.; Balakrishnan, G.; Lees, M. R. Multigap superconductivity in chiral noncentrosymmetric $TaRh_2B_2$. *Phys. Rev. B* **2018**, *98*, No. 014502.
(15) Mayoh, D. A.; Pearce, M. J.; Götze, K.; Hillier, A. D.; Balakrishnan, G.; Lees, M. R. Superconductivity and the upper critical field in the chiral noncentrosymmetric superconductor $NbRh_2B_2$. *J. Phys. Condens. Matter.* **2019**, *31*, No. 465601.
(16) Matano, K.; Ogura, R.; Fountaine, M.; Jeschke, H. O.; Kawasaki, S.; Zheng, G. Q. Antiferromagnetic spin fluctuations and superconductivity in $NbRh_2B_2$ and $TaRh_2B_2$ with a chiral crystal structure. *Phys. Rev. B* **2021**, *104*, No. 224508.
(17) Arumugam, S.; Subbulakshmi, N.; Manikandan, K.; Kannan, M.; Mayoh, D. A.; Lees, M. R.; Balakrishnan, G. Investigation of the transport, magnetic and flux pinning properties of the non-centrosymmetric superconductor $TaRh_2B_2$ under hydrostatic pressure. *Phys. C Supercond. Appl.* **2020**, *571*, No. 1353586.
(18) Drozdov, A. P.; Eremets, M.; Troyan, A., II.; Ksenofontov, V.; Shylin, S. I. Conventional superconductivity at 203 kelvin at high pressures in the sulfur hydride system. *Nature* **2015**, *525*, 73−76.
(19) Troyan, I. A.; Semenok, D. V.; Kvashnin, A. G.; Sadakov, A. V.; Sobolevskiy, O. A.; Pudalov, V. M.; Ivanova, A. G.; Prakapenka, V. B.; Greenberg, E.; Gavriliuk, A. G.; Lyubutin, I. S.; Struzhkin, V. V.; Bergara, A.; Errea, I.; Bianco, R.; Calandra, M.; Mauri, F.; Monacelli, L.; Akashi, R.; Oganov, A. R. Anomalous high temperature superconductivity in YH_6. *Adv. Mater.* **2021**, *33*, No. 2006832.
(20) Kong, P.; Minkov, V. S.; Kuzovnikov, M. A.; Drozdov, A. P.; Besedin, S. P.; Mozaffari, S.; Balicas, L.; Balakirev, F. F.; Prakapenka, V. B.; Chariton, S.; Knyazev, D. A.; Greenberg, E.; Eremets, M. I. Superconductivity up to 243 K in the yttrium-hydrogen system under high pressure. *Nat. Commun.* **2021**, *12*, 5075.
(21) Snider, E.; Dasenbrock-Gammon, N.; McBride, R.; Debessai, M.; Vindana, H.; Vencatasamy, K.; Lawler, K. V.; Salamat, A. Dias Room-temperature superconductivity in a carbonaceous sulfur hydride. *Nature* **2020**, *586*, 373−377.
(22) Gor'kov, L. P.; Kresin, V. Z. Colloquium: High pressure and road to room temperature superconductivity. *Rev. Mod. Phys.* **2018**, *90*, No. 011001.
(23) Peng, F.; Sun, Y.; Pickard, C. J.; Needs, R. J.; Wu, Q.; Ma, Y. Hydrogen clathrate structures in rare earth hydrides at high pressures: Possible route to room-temperature superconductivity. *Phys. Rev. Lett.* **2017**, *119*, No. 107001.
(24) Sukmas, W.; Tsuppayakorn-aek, P.; Pinsook, U.; Bovornratanaraks, T. Near-room-temperature superconductivity of Mg/Ca substituted metal hexahydride under pressure. *J. Alloys Compd.* **2020**, *849*, No. 156434.
(25) Wang, C.; Yi, S.; Cho, J. H. Multiband nature of room-temperature superconductivity in LaH_{10} at high pressure. *Phys. Rev. B* **2020**, *101*, No. 104506.
(26) Verma, A. K.; Modak, P.; Schrodi, F.; Aperis, A.; Oppeneer, P. M. Phonon-mode specific contributions to room-temperature superconductivity in atomic hydrogen at high pressures. *Phy Rev B* **2021**, *103*, No. 094505.
(27) Wang, T.; Hirayama, M.; Nomoto, T.; Koretsune, T.; Arita, R.; Flores-Livas, J. A. Absence of conventional room-temperature superconductivity at high pressure in carbon-doped H_3S. *Phys. Rev. B* **2012**, *104*, No. 064510.
(28) Mariappan, S.; Krishnan, M.; Bhoi, D.; Ma, H.; Gouchi, J.; Motla, K.; Singh, R. P.; Vajeeston, P.; Sonachalam, A.; Uwatoko, Y. Superconducting and structural properties of the noncentrosymmetric Re_6Hf superconductor under high pressure. *Phys. Rev. B* **2022**, *105*, No. 224505.
(29) Islam, J.; Farjana, N.; Islam, M. D.; Shabnam, S.; Rahman, M. A. Effect of Pressure on the Superconducting Transition Temperature and Physical Properties of $CaPd_2P_2$: A DFT Investigation. *ACS Omega* **2022**, *7*, 21528−21536.
(30) Hohenberg, P.; Kohn, W. Inhomogeneous electron gas. *Phys. Rev. B* **1964**, *136*, 864−871.
(31) Kohn, W.; Sham, L. J. Self-consistent equations including exchange and correlation effects. *Phys. Rev. A* **1965**, *140*, 1133−1138.
(32) Clark, S. J.; Segall, M. D.; Pickard, C. J.; Hasnip, P. J.; Probert, M. I. J.; Refson, K.; Payne, M. C. First principles methods using CASTEP. *Z Kristallogr. Cryst. Mater.* **2005**, *220*, 567−570.
(33) Perdew, J. P.; Burke, K.; Ernzerhof, M. Generalized gradient approximation made simple. *Phys. Rev. Lett.* **1996**, *77*, 3865−3868.
(34) Vanderbilt, D. Soft self-consistent pseudopotentials in a generalized eigenvalue formalism. *Phys. Rev. B* **1990**, *41*, 7892−7895.
(35) Monkhorst, H. J.; Pack, J. D. Special points for Brillouin-zone integrations. *Phys. Rev. B* **1976**, *13*, 5188−5192.
(36) Fischer, T. H.; Almlof, J. General methods for geometry and wave function optimization. *J. Phys. Chem. A* **1992**, *96*, 9768−9774.
(37) Born, M.; Huang, K.; Lax, M. Dynamical theory of crystal lattices. *Am. J. Phys.* **1955**, *23*, 474−474.

https://doi.org/10.1021/acsomega.3c01461
ACS Omega 2023, 8, 21813−21822

(38) Mouhat, F.; Coudert, F.-X. Necessary and sufficient elastic stability conditions in various crystal systems. *Phys. Rev. B* **2014**, *90*, No. 224104.
(39) SinKo, G. V.; Smirnov, N. A. Ab initio calculations of elastic constants and thermodynamic properties of bcc, fcc, and hcp Al crystals under pressure. *J. Phys. Condens. Matte.* **2002**, *14*, 6989.
(40) Gao, J.; Zeng, W.; Tang, B.; Fan, D. H.; Liu, Q. J.; Chang, X. H.; Zhong, M. Effects of pressure on structural, mechanical, and electronic properties of trigonal and monoclinic $MgSiO_3$. *Solid Stat. Sci.* **2020**, *105*, No. 106261.
(41) Ohno, I.; Yamamoto, S.; Anderson, O. L.; Noda, J. Determination of elastic constants of trigonal crystals by the rectangular parallelepiped resonance method. *J. Phys. Chem. Solids* **1986**, *47*, 1103−1108.
(42) Mayer, W. G.; Hiedemann, E. A. Corrected values of the elastic moduli of sapphire. *J. Acoust. Soc. Am.* **1960**, *32*, 1699−1700.
(43) Heyliger, P.; Ledbetter, H.; Kim, S. Elastic constants of natural quartz. *J. Acoust. Soc. Am.* **2003**, *114*, 644−650.
(44) Bernstein, B. T. Elastic constants of synthetic sapphire at 27 C. *J. Appl. Phys.* **1963**, *34*, 169−172.
(45) Gieske, J. H.; Barsch, G. R. Pressure dependence of the elastic constants of single crystalline aluminum oxide. *Phys. Status Solidi B* **1968**, *29*, 121−131.
(46) Wachtman, J. B.; Tefft, W. E.; Lam, D. G.; Stinchfield, R. P. J. *Res natn Bur Stand* **1960**, *64A*, 213.
(47) Karim, A.; Hadi, M. A.; Alam, M. A.; Parvin, F.; Naqib, S. H.; Islam, A. K. M. A. Newly synthesized $MgAl_2Ge_2$: A first principles comparison with its silicide and carbide counterparts. *J. Phys. Chem. Solids* **2018**, *117*, 139−147.
(48) Parvin, F.; Naqib, S. H. Pressure dependence of structural, elastic, electronic, thermodynamic, and optical properties of van der Waals-type $NaSn_2P_2$ pnictide superconductor: insights from DFT study. *Results Phys.* **2021**, *21*, No. 103848.
(49) Pettifor, D. G. Theoretical predictions of structure and related properties of intermetallics. *Mater. Sci. Technol.* **1992**, *8*, 345−349.
(50) Voigt, W. Lehrbuch der Kristallphysik, Leipzig, Taubner. *Adv. Earth Sci.* **1928**, *1*, 1−978.
(51) Reuss, A. Berechnung der Fließgrenze von Mischkristallen auf Grund der Plastizitatsbedingung fur Einkristalle. *Z. Angew. Math Mech.* **1929**, *9*, 49−58.
(52) Hill, R. The elastic behaviour of a crystalline aggregate. *Proc. Phys. Soc. A* **1952**, *65*, 349−354.
(53) Pugh, S. F. XCII. Relations between the elastic moduli and the plastic properties of polycrystalline pure metals. *Lond. Edinb. Dublin Philos. Mag. J. Sci.* **1954**, *45*, 823−843.
(54) Frantsevich, I. N.; Voronov, F. F.; Bakuta, S. A. *Handbook on Elastic Constants and Moduli of Elasticity for Metals and Nonmetals*; Naukova Dumka: Kiev, 1982.
(55) Anderson, O. L.; Demarest, H. H. Elastic constants of the central force model for cubic structures: Polycrystalline aggregates and instabilities. *J. Geophys. Res.* **1971**, *76*, 1349−1369.
(56) Fine, M. E.; Brown, L. D.; Marcus, H. L. Elastic constants versus melting temperature in metals. *Scr. Metall.* **1984**, *18*, 951−956.
(57) Anderson, O. L. A simplified method for calculating the Debye temperature from elastic constants. *J. Phys. Chem. Solids* **1963**, *24*, 909−917.
(58) McMillan, W. L. Transition temperature of strong-coupled superconductors. *Phys. Rev.* **1968**, *167*, 331−344.
(59) Kholil, M. I.; Ali, M. S.; Aftabuzzaman, M. Structural, elastic, electronic and vibrational properties of $BaRh_2P_2$ and $SrIr_2As_2$ superconductors: a DFT study. *J. Alloys Compd.* **2018**, *740*, 754−765.
(60) Khan, N. S.; Rano, B. R.; Syed, I. M.; Islam, R. S.; Naqib, S. H. First-principles prediction of pressure dependent mechanical, electronic, optical, and superconducting state properties of NaC_6: A potential high-T_c superconductor. *Results Phys* **2022**, *33*, No. 105182.
(61) Blawat, J.; Swatek, P. W.; Das, D.; Kaczorowski, D.; Jin, R.; Xie, W. Pd-P antibonding interactions in APd_2P_2 (A = Ca and Sr) superconductors. *Phys. Rev. Mater.* **2020**, *4*, No. 014801.

https://doi.org/10.1021/acsomega.3c01461
ACS Omega 2023, 8, 21813−21822